Lyu, S.; Zheng, R.; Xiao, W.; Huang, Y.; Gavras, S.; Hort, N.; Li, G.; Ma, C.:
Abnormal extrusion texture and reversed yield asymmetry in a Mg–Y-Sm-Zn-Zr alloy.
In: Materials Science and Engineering A. Vol. 760 (2019) 426 - 430.
First published online by Elsevier: 10.06.2019

https://dx.doi.org/10.1016/j.msea.2019.06.029

Abnormal extrusion texture and reversed yield asymmetry in a Mg-Y-Sm-Zn-Zr alloy

Shaoyuan Lyu [a, b], Ruixiao Zheng [a*], Wenlong Xiao [a*], Yuanding Huang [b],

Serge Gavras [b], Norbert Hort [b], Guodong Li [a], Chaoli Ma [a]

[a] *Key Laboratory of Aerospace Advanced Materials and Performance of Ministry of Education, School of Materials Science and Engineering, Beihang University, Beijing 100191, China*

[b] *MagIC-Magnesium Innovation Centre, Helmholtz-Zentrum Geesthacht, Max-Planck-Str. 1, 21502 Geesthacht, Germany*

* Corresponding author: Tel: +86-10-8233 8631; Fax: +86-10-8233 8631

E-mail: zhengruixiao@buaa.edu.cn (R.X. Zheng);

wlxiao@buaa.edu.cn (W. L. Xiao)

Abstract

An extruded Mg-Y-Sm-Zn-Zr alloy exhibited an abnormal texture component, that is, the ***c***-axis of most grains was aligned parallel to the extrusion direction. The reversed yield asymmetry with a tension/compression of 0.94 was attributed to the activation of extension twinning under tensile strain.

.

Keywords: Magnesium alloys; Texture; Twinning; Work hardening; Yield asymmetry

1. Introduction

Extruded magnesium (Mg) and its alloys have attracted significant attention in the past several decades. However, due to their highly anisotropic hexagonal close-packed (HCP) crystal structure, extruded Mg alloys exhibit an undesirable yield asymmetry.

The yield strength in compression along the extrusion direction (ED) is always much lower than that in tension [1-2]. The origins of such phenomenon are attributed to the combination of a strong fiber texture after extrusion (***c***-axis perpendicular to the ED) and the asymmetric nature of deformation twinning in Mg. The $\{10\bar{1}2\}$ extension twinning is activated easily in compression along the ED but not in tension [1].

Many efforts have been made to reduce the yield asymmetry through texture modification [3-4]. Additions of rare earth (RE) elements to Mg alloys were considered as one of the best approaches to modify the textures [5]. Stanford *et al*. [6] found that the addition of Gd (1.55 wt %) to pure Mg can effectively reduce the angle between the ***c***-axis and ED from 90° (pure Mg) to 60°. Li *et al.* [7] showed that the volume fraction of grains having their ***c***-axis parallel to the ED increased from 4.0% to 15.5% after annealing in an extruded Mg-14Gd-2Ag-0.5Zr alloy. They claimed that the unique texture evolution during annealing was related to the different stored energy and grain boundary misorientation. Moreover, extrusion parameters, such as the extrusion ratio and temperature also affect the texture evolution [8]. Alizadeh *et al*. [9] reported that the fraction of grains with ***c***-axis parallel to the ED increased with increasing the extrusion ratio in a Mg-9Gd-4Y-0.4Zr alloy, but the reason for this remained unclear. Though the abnormal texture was observed in the above-mentioned alloys, the texture intensity was weak and the grain volume fraction with *c*-axis parallel to ED was less than 20%. The low cost of Sm and high aging-hardening effect of Mg-Sm-Zn-Zr alloy [10] was the motivation to investigate this alloy system in order to replace the high-cost Mg-Gd/Y based alloy. However, the moderate solubility of Sm in α-Mg (<5.8 wt.%) limits the further improvement in strength of Mg alloys by age strengthening. Therefore, replacing part of Gd/Y by Sm in high-strength Mg-RE alloys may be a viable solution. Li *et.al* [11] cast a Mg-4Y-4Sm-0.5Zr alloy, whose mechanical properties are better than those of WE54 alloy, though the alloy has less RE content. Hence, a Mg-Y-Sm-Zn-Zr alloy was selected. Interestingly, an abnormal extrusion texture, with most of the grains having their ***c***-axis parallel to the ED, was obtained in a newly designed Mg-Y-Sm-Zn alloy after hot extrusion. This was different from previous results, a reversed yield asymmetry was found when tested along the ED. The reasons for the formation of such

abnormal extrusion texture and reversed yield asymmetry phenomenon were investigated.

2. Material and methods

The investigated alloy with a nominal composition of Mg-7Y-5Sm-0.5Zn-0.3Zr (wt.%) was prepared from high purity Mg and Zn (⩾99.9%), Mg-30%Y, Mg-20%Sm and Mg-30%Zr master alloys in an electrical resistance furnace under an Ar gas protective atmosphere. The actual composition was Mg-6.91Y-4.21Sm-0.60Zn-0.19Zr measured by an inductively coupled plasma atomic emission spectroscopy analyzer (ICP). The as-cast ingot was solution-treated at 495 °C for 12 hrs and then was machined into cylinders with a diameter of 40 mm and height of 20 mm. The indirect extrusion was performed at 420 °C with an extrusion ram speed of 1.8 mm/s and an extrusion ratio of 16. Finally, an extrusion rod with diameter 10 mm was produced.

The microstructures were characterized by optical microscopy (OM), field emission scanning electron microscopy (FE-SEM) using an Apollo-300 equipped with an electron backscattering diffraction (EBSD) system and a JEM-2100F transmission electron microscopy (TEM). The grain sizes of the alloy was measured using the linear line intercept method. The tensile specimens with a gauge length of 18 mm, a diameter of 4 mm and compressive specimens with a height of 8 mm, a diameter of 4 mm, were prepared from the extruded bars along the ED. Mechanical properties were characterized by uniaxial tensile and compressive tests with a strain rate of 5.0×10^{-4} s^{-1} at room temperature. Another set of tests were interrupted when the strain was 3.0 % and 4.2 % for tension and compression, respectively (deformed sample). At least three tests were performed for each condition.

3. Results

OM images of the as-extruded alloy are shown in **Fig. 1 (a)** and **(b)**. Equiaxed grains with a mean grain size of 11 ± 0.8 μm and a small fraction of irregular-shaped particles are clearly observed. Parallel lamellae are found in the majority of the grains, except in some of the brighter contrasted ones (**Fig. 1 (b)**). Higher resolution SEM

micrograph of these lamellae is shown in **Fig. 1 (c)**. All the lamellae within one grain have the same orientation but vary significantly from one grain to another, as marked by the red arrows. Further TEM observations (**Fig. 1 (d)**) identified that the lamellae within the grains have a 14H long period stacking ordered (LPSO) phase.

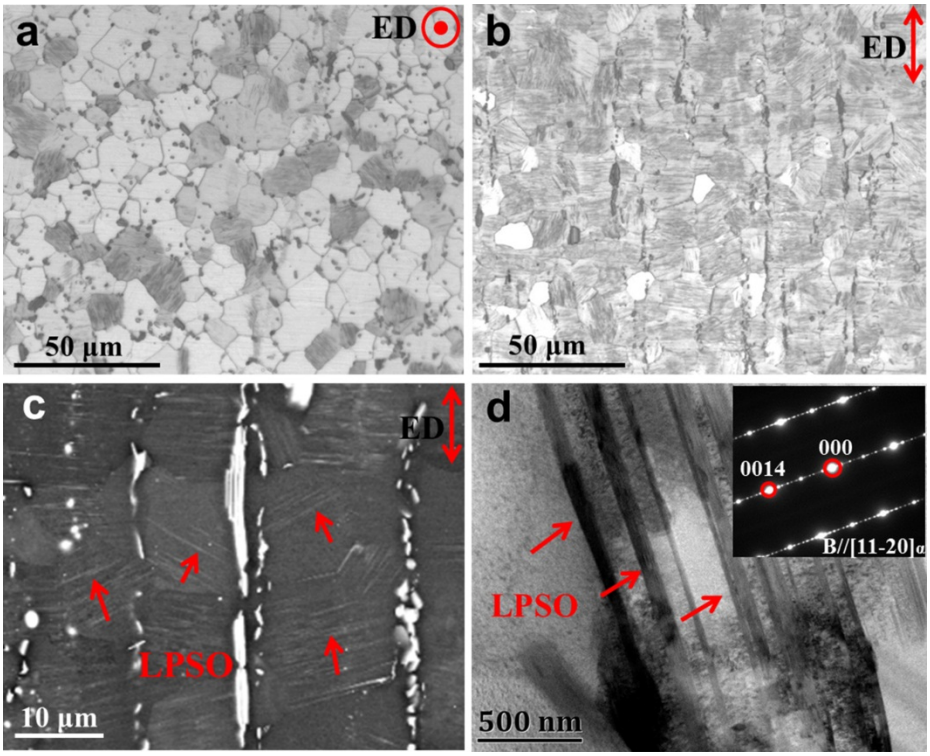

Fig. 1 OM micrograph (a) and SEM micrograph (b, c) of the Mg-Y-Sm-Zn-Zr alloy and (d) TEM bright field micrograph of LPSO and corresponding SAED observed from$[11\bar{2}0]$ direction.

Fig. 2(a) shows the inverse pole figures (IPF) map of Mg-Y-Sm-Zn-Zr alloy. Most grains appear in red, suggesting the ***c***-axis orientations of these grains are close to the extrusion direction (ED). The corresponding (0001) pole figure and inverse pole figure in **Fig. 2(b)** confirmed the existence of a strong abnormal extrusion texture (I_{max}=17.1), which is clearly different from that in the as-extruded pure Mg and other Mg-RE alloys [6,12]. A schematic illustration showing distribution of the hexagonal unit cell in the extruded pure Mg, conventional Mg-RE alloys and the Mg-Y-Sm-Zn-Zr alloy is depicted in **Fig. 2 (c)**. Generally, it was accepted that the addition of RE elements in magnesium could weaken or even change their basal texture. In the present investigation, following a review of the literature, it is the first time to observe such a

high volume fraction ratio of grains with their ***c***-axis parallel to the ED.

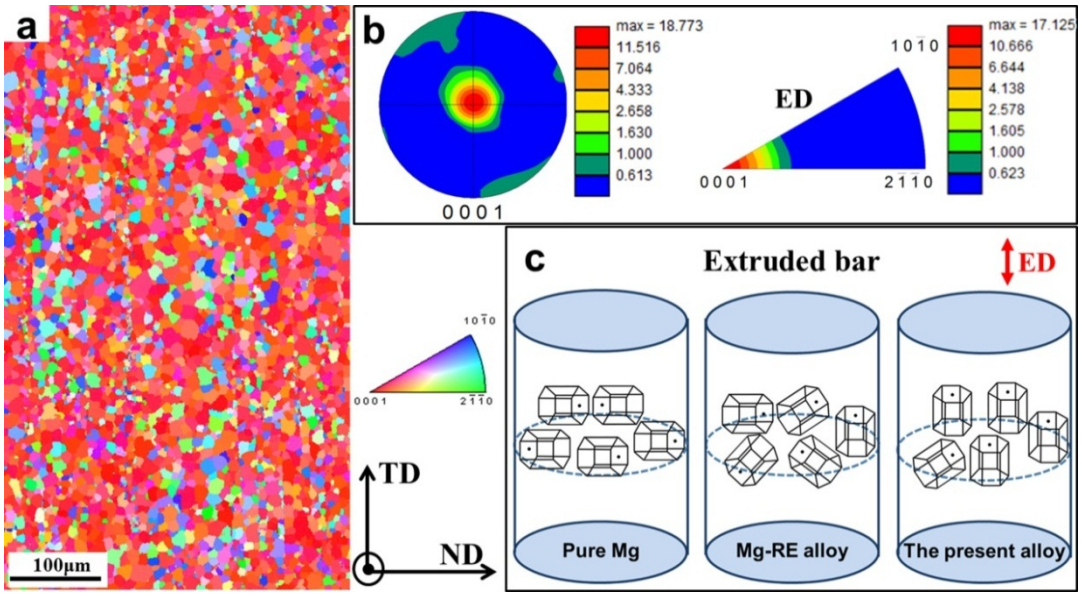

Fig. 2 EBSD inverse pole figure (IPF) map of the Mg-Y-Sm-Zn-Zr alloy (a) and corresponding (0001) pole figure and inverse pole figure (b). In (c), schematic diagrams of hexagonal unit cells in extruded pure Mg, conventional Mg-RE alloy [6, 12] and Mg-Y-Sm-Zn-Zr alloy.

4. Discussion

4.1 Formation mechanisms of the abnormal texture

The formation of this abnormal texture is attributed to three underlying mechanisms. Firstly, the RE atoms segregate at grain boundaries, especially for high RE content alloys. The solute segregation at grain boundaries or dislocation core and the slow diffusivity of RE atoms in Mg impede the migration of grain boundaries and movement of dislocations via solute drag [13-14], which leads to texture modifications. Secondly, the sufficient energy to allow growth of the specific orientation is necessary. Alizadeh *et. al* [9] found that high a extrusion ration would produce a <0001>//ED texture by changing the nucleation sites of recrystallization compared to a low extrusion ratio. Li *et.al* [7] also confirmed that the fraction of grains with <0001>//ED orientation increased with the increasing annealing time. Thus, the growth of certain orientations was promoted by providing sufficient energy in both of the alloys. Thirdly, the deformation modes are changed during extrusion. At extrusion temperature, the differences of critical resolved shear stresses (CRSS) between basal slip and non-basal

slip decrease significantly [15]. Furthermore, large numbers of precipitates (LPSO and γ') on the basal plane of present alloy [16] will improve the CRSS of basal slip [17]. This would impede the dislocation mobility in the basal plane and activate the non-basal slip at the interface between the precipitate and the α-Mg matrix. The Schmid factor (SF) distributions with respect to the basal, prismatic, and pyramidal <*c*+*a*> slip planes of the sample in the extrusion deformation zone illustrate that the possibility of prismatic and pyramidal slip is higher than basal slip during hot extrusion (**Fig. 3)**. In addition, it is reported that blocky LPSO phases would induce the <0001>//ED texture during extrusion process, but in present alloy, the influence is negligible due to the small number of block-shaped LPSO [18]. Moreover, the fine plate-shaped LPSO phase can stimulate <1010>// ED fiber texture evolution [19], which is not consistent with that in present alloy. Note that the <0001>//ED texture was also generated in previous Mg-RE alloys without LPSO and Zn addition [7-9]. Therefore, it is inferred that the formation of abnormal texture is mainly attributed to the high strain and high RE content.

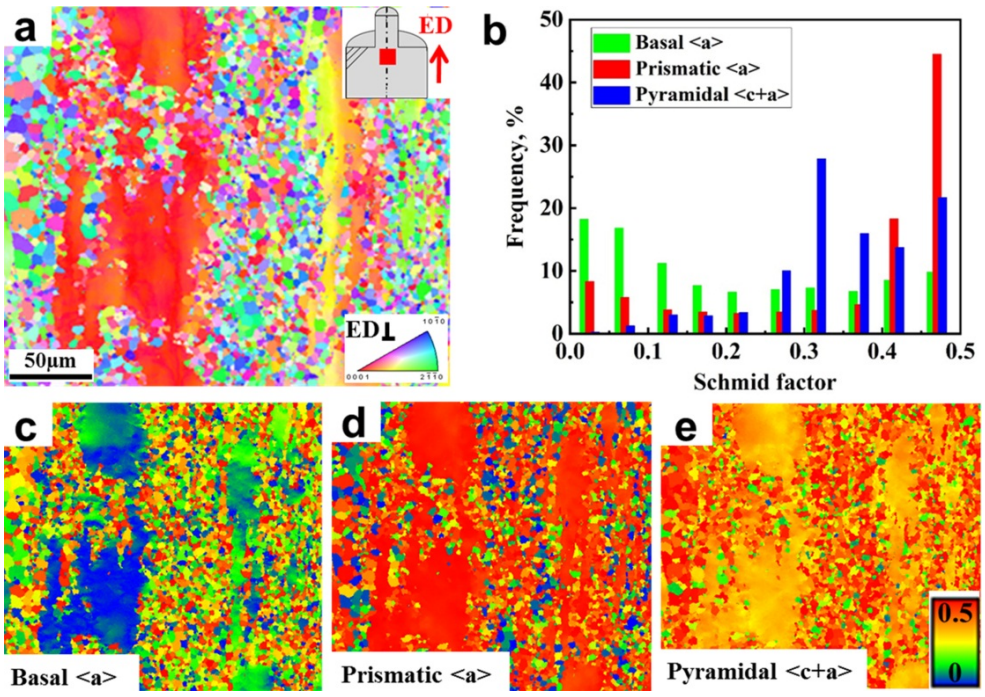

Fig. 3 (a) EBSD inverse pole figure (IPF) maps of the red area in deformation zone. Schmid factor (SF) distributions (b) and SF maps with respect to various slip systems: (c) Basal <a>: {0001}<11$\bar{2}$0>, (d) Prismatic <a>: {1010}<11$\bar{2}$0>, (e) Pyramidal <c+a>: {11$\bar{2}$2}<11$\bar{2}$3>.

4.2 Yield asymmetry of the extruded alloy

Typical engineering stress-strain curves of the extruded alloy are presented in **Fig. 4 (a)**. Note that the slope of the elastic region in the compressive curve is much lower than that of the tensile curve, due to the extensometer not being used in the compression test. It is very interesting that the tensile yield strength (TYS; 0.2% offset stress) and compressive yield strength (CYS) are 242 ± 6 MPa and 257 ± 5 MPa, respectively, resulting in a yield ratio (TYS/CYS) of 0.94, which is opposite to that in typical extruded Mg alloys (TYS/CYS＞1). After yielding, both curves exhibit clear work hardening upon plastic deformation. **Fig. 4 (b)** shows the work hardening rate ($\Theta = \left(\frac{\partial \sigma}{\partial \varepsilon}\right)_{\dot{\varepsilon}}$, where σ and ε are the true stress and true strain, respectively [20]) plotted against true strain. For compression testing, the work hardening rate decreased monotonically with the increase of true strain. A clear discontinuous work hardening behavior at low strain is observed under tension testing. The Θ decreased sharply at the beginning of plastic deformation, followed by an increase of the Θ upon further tensile deformation, resulting in a V-shaped valley at low strains. After that, the Θ decreased monotonically with a much lower slope than that of the compression curve.

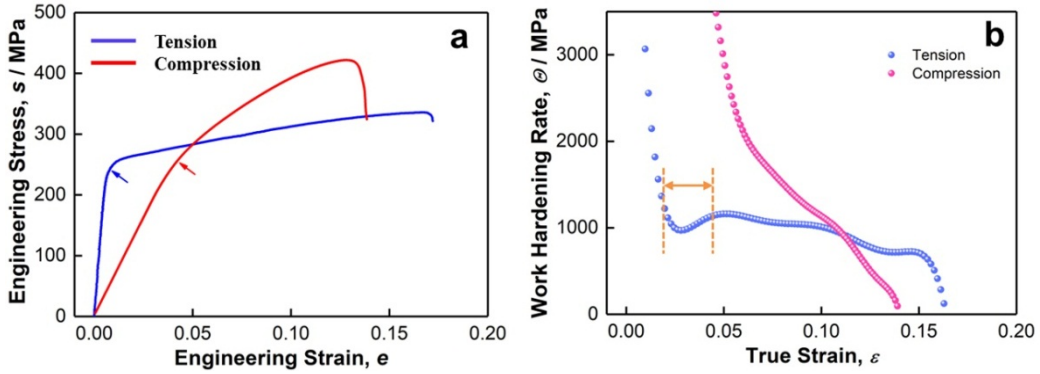

Fig. 4 (a) Typical engineering stress-strain curves and (b) work hardening rate against the true strain of the extruded alloy in tension and compression.

It is well known that the low CYS in extruded Mg alloys is attributed to the ease of formation and propagation of $\{10\bar{1}2\}$ extension twins [1]. Although a clear plateau is not observed in the present stress-strain curves (**Fig. 4 (a)**), it is considered that the V-shaped change of the work hardening rate under tension is likely related to the

enhanced activity of deformation twinning. **Fig. 5 (a-d)** shows EBSD results of an identical area before and after tensile deformation to a plastic strain of 3.0%. The color in the IPF maps (**Fig. 5 (a, b)**) indicates crystallographic orientations parallel to the ED of the specimen. **Fig. 5 (c)** shows the corresponding grain boundary (GB) map superimposed on band contrast where the blue, green and red lines correspond to high angle grain boundaries with misorientations larger than 15°, low angle grain boundaries (LAGBs) with misorientations between 2° and 15° and twin boundaries (TB), respectively. **Fig. 5 (d)** is the IPF map extracting only deformation twins. At a tensile strain of 3%, significant amounts of lenticular-shaped deformation twins with an area fraction of 2.8% were generated. Crystallographic analysis indicated that these twins were all $\{10\bar{1}2\}$ extension twins, which rotates the lattice around the $\langle 1\bar{1}20\rangle$ direction by 86° so as to accommodate extension deformation along ***c***-axis significantly [21]. All the twin lamellae appear as blue or green in **Fig. 5 (d)**, suggesting that the ***c***-axis of the twins was close to the direction perpendicular to the ED. In other words, the grains, whose ***c***-axis were nearly parallel to the ED, tended to show $\{10\bar{1}2\}$ extension twins under tensile testing. An identical area EBSD observation was also conducted before and after compressive deformation to a plastic strain of 4.2%, as shown in **Fig. 5 (e-h)**. As shown in **Fig. 5 (h)**, a quite limited number of deformation twins with an area fraction of only 0.7% formed, which was significantly lower than that of the tensile test (2.8%). In this case, all the twin lamellae appeared in red, indicating that the ***c***-axis of the twins was close to the direction parallel to the ED. Therefore, it is concluded that the reversed yield asymmetry (TYS/CYS＜1) was mainly induced by the abnormal extrusion texture, which led to the enhanced activity of $\{10\bar{1}2\}$ extension twinning under tensile testing along ED. Moreover, due to the relatively low amount, the influence of blocky LPSO on yield asymmetry could be neglected. The reduced tension-compression asymmetry (TYS/CYS=0.94) is mainly affected by the suppression of the activity of twinning. The twining formation and growth are impeded by the following factors: 1) High Y content could increase the stress requirement to activate the {10-12} twin, due to the large Y atomic radius, which inhibits the atomic shuffling process accompanying twinning shear [22]; 2) The lamellar LPSO in grain interior also acted

as a barrier to restrain the formation of twinning by improving the energy requirement to kink the intercepting lamellar LPSO phase [23]; 3) The small size of grains in present extruded alloy would hinder the formation of twins [24]. All these factors give rise to a relatively high yield symmetry in present alloy.

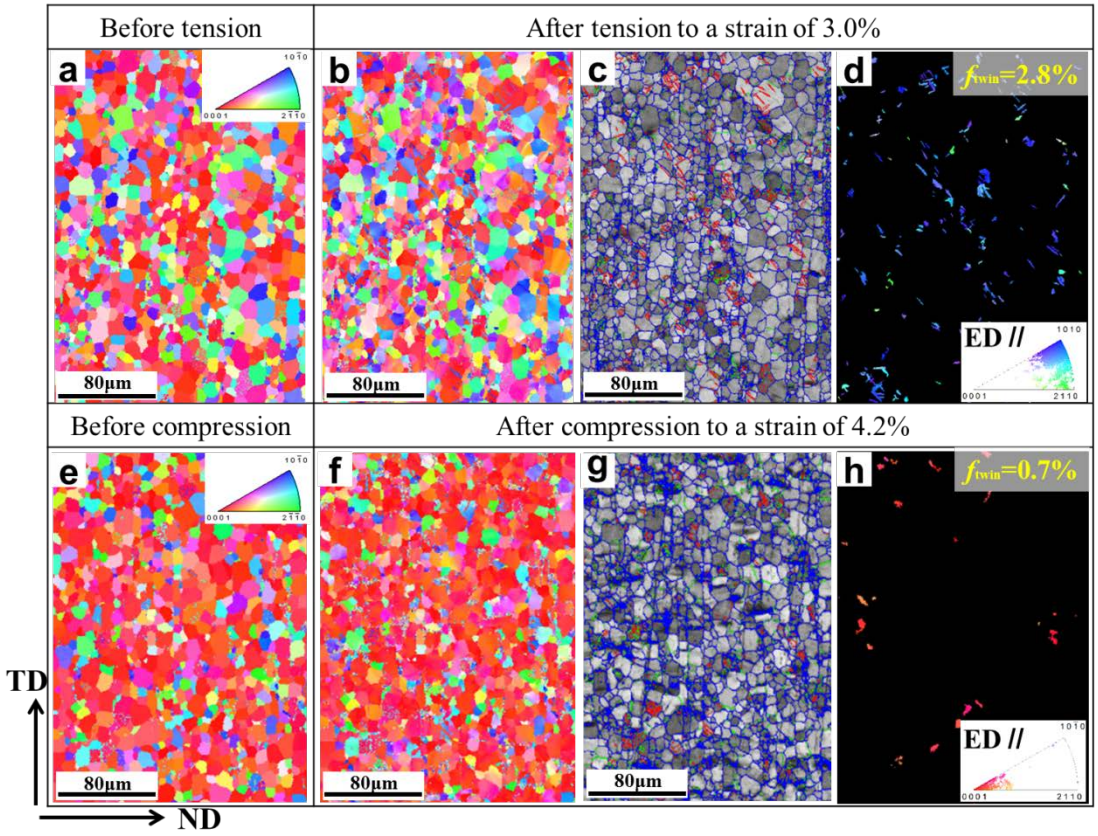

Fig. 5 EBSD maps for tension (a-d) and compression (e-f). (identical area to the region prior deformation).

4. Conclusion

In summary, an abnormal extrusion texture was found in an Mg-Y-Sm-Zn-Zr alloy. The ***c***-axis of most of the grains were aligned parallel to the ED after hot extrusion. The extruded alloy exhibited a reversed yield asymmetry due to the activation of extension twins during tensile testing, while the relatively high yield symmetry (TYS/CYS=0.94) was attributed to the suppression of twinning by lamellar LPSO in the grain interior. The present results can broaden our knowledgebase to design new Mg alloys with controllable texture to enhance their formability and performance.

Statement

The raw/processed data required to reproduce these findings cannot be shared at this time as the data also forms part of an ongoing study.

Acknowledgments

This work was financially supported by the National Key Research and Development Program of China (No. 2016YFB0301103) and National Natural Science Foundation of China (NSFC, No. 51401010). S.Y. Lyu would like to thank China Scholarship Council (CSC) fund.

References

[1] E.A. Ball, P. B. Prangnell, Scr. Mater. 31 (1994) 111-116.

[2] D. Yin, J. Wang, J. Liu et.al, J. Alloy. Compd. 478 (2009) 789-795.

[3] N. Stanford, M. Barnett, Scr. Mater. 58 (2008) 179-182.

[4] J.D. Robson, A.M. Twier, G.W. Lorimer et.al, Mater. Sci. Eng. A 528 (2011) 7247-7256.

[5] K. Hantzsche, J. Bohlen, J. Wendt et.al, Scr. Mater. 63 (2010) 725-730.

[6] N. Stanford, M.R. Barnett, Mater. Sci. Eng. A 496 (2008) 399-408.

[7] R. Li, J. Zhang, G. Fu et.al, Adv. Eng. Mater. 20(2018)1701129–1-5.

[8] S.H. Kim, J.G. Jung, B.S. You et.al, J. Alloy. Compd. 695 (2017) 344-350.

[9] R. Alizadeh, R. Mahmudi, Alfonso H. et.al, Adv. Eng. Mater. 18(2016) 1044-1049.

[10] X.Y. Xia, W.H. Sun, A.A. Luo et.al, Acta Mater. 111 (2016) 335-347.

[11] D.Q. Li, Q.D. Wang, W.J. Ding, Mater. Sci. Eng. A 448 (2007) 165-170.

[12] B. Wu, Y. Zhao, X. Du et.al, Mater. Sci. Eng. A 527 (2010) 4334-4340.

[13] S.K. Das, Y.B. Kang, T. Ha et.al, Acta Mater. 71(2014) 164-175

[14] J.P. Hadorn, T.T. Sasaki, T. Nakata et.al, Scr. Mater. 93 (2014) 29-31.

[15] M.R. Barnett, Metall. Mater. Trans. A 34(2003)1799-1806.

[16] S. Lyu, W. Xiao, R. Zheng et.al, Mater. Sci. Eng. A 732 (2018) 178-185.

[17] K. Hagihara, Z.X. Li, M. Yamasaki et.al, Acta Mater. 163 (2019) 226-239.

[18] L. Tong, X. Li, H. Zhang, Mater. Sci. Eng. A 563(2013) 177-183

[19] Y. Jono, M. Yamasaki, Y. Kawamura, Mater. Trans. 54 (2013) 703-712.

[20] G.E. Dieter, D. Bacon, Mechanical Metallurgy, McGraw-Hill, New York, 1986.

[21] S. Kleiner, P.J. Uggowitzer, Mater. Sci. Eng. A 379 (2004) 258-263.

[22] N. Stanford, R.K.W. Marceau, M.R. Barnett, Acta Mater. 82 (2015), 447-456.

[23] T. Chen, Z. Chen, J. Shao et.al, Mater. Sci. Eng. A 750 (2019) 31-39.

[24] M.R. Barnett, Scr. Mater. 59 (2008) 696-698.